Compact Modeling and System Implications of Microring Modulators in Nanophotonic Interconnects

Rui Wu[1], Chin-Hui Chen[2], Jean-Marc Fedeli[3], Maryse Fournier[3],
Raymond G. Beausoleil[2], and Kwang-Ting Cheng[1]
[1]Department of Electrical & Computer Engineering, University of California, Santa Barbara, CA, US
[2]HP Labs, Hewlett-Packard Company, Palo Alto, CA, US
[3]CEA, LETI, Minatec Campus, Grenoble, France
ruiwu@ece.ucsb.edu, chin-hui.chen@hp.com, {jean-marc.fedeli, maryse.fournier}@cea.fr
ray.beausoleil@hp.com, timcheng@ece.ucsb.edu

ABSTRACT

Silicon microring modulators are critical components in optical on-chip communications. In this paper, we develop theoretical compact models for optical transmission, power consumption, bit-error-rate (BER), and electrical tuning of microring modulators. The proposed theoretical models have been extensively validated by fabricated devices from a number of designs and fabrication batches. Since the quality factor (Q) and the extinction ratio (ER) of the microring modulator are important to determine the BER and link power budget, we include accurate equations for the Q and the ER in our models. Based on the proposed models, we identify an extra power penalty for the electrical tuning, and an energy-efficient swing voltage for the microring modulator to achieve to minimum total energy consumption.

1. INTRODUCTION

Providing intrinsically high bandwidth and low latency, nanophotonic interconnects have been recognized as a promising alternative to traditional electrical interconnects that suffer from large delay and high power dissipation, especially for long wires [1]. To support system-level simulations of large-scale nanophotonic interconnect systems, accurate compact behavior models for photonic devices are desirable. Much industrial efforts have been paid to developing and standardizing transmission spectrum models for photonic devices (e.g., Synopsys' RSoft OptSim Circuit [2], Lumerical's INTERCONNECT integrated with Mentor Graphics' tools [3], Si2 Silicon Photonics TAB's Open Matrices [4]).

Microring modulators are widely used in wavelength-division multiplexing (WDM) nanophotonic interconnects because of its high wavelength-selectivity, small footprint, and power-efficiency. It is imperative to develop accurate compact models for microring modulators. The resonance wavelength λ_r shift of the microring modulator is essential for the on-off keying modulation. Therefore, we derive an theoretical equation for the resonance wavelength shift based on physical principles. The proposed model greatly improves the fitting accuracy compared to the empirical models in [5, 6]. Additionally, the quality factor $\mathbb{Q}$ and extinction ratio ER of the microring modulator are important in determining the link power budget and BER [7]. Meanwhile, the $\mathbb{Q}$ and the ER change significantly with bias conditions. However, the $\mathbb{Q}$ and the ER are not included in many existing models for microring modulators [5, 6, 8–12]. Thus, we propose theoretical equations for the $\mathbb{Q}$ and the ER with bias conditions, which are consistent with the measurement data. In summary, the models for λ_r, $\mathbb{Q}$ and ER together result in an accurate description of the optical transmission spectrum of the microring modulator.

We have fabricated batches of carrier-injection microring modulators with various designs at the CEA LETI foundry (Fig. 1). The optical transmission spectrum of fabricated devices are measured with various bias conditions. Our proposed theoretical models for λ_r, $\mathbb{Q}$ and ER are extensively validated by the measured data of devices from various designs and fabrication batches.

Based on the validated optical spectrum models, we further propose analytical models for power consumption, BER, and electrical tuning of microring modulators. The BER model shows that the bit-error-rate (BER) depends on the the $\mathbb{Q}$ and the ER. Furthermore, an extra power penalty is identified and include in the electrical tuning model. By using the proposed models, we also explore the design tradeoffs between the modulation energy and laser power, which shows an energy-efficient AC swing voltage minimizing the total energy consumption per bit.

Overall, the main contributions of this paper are:

- Develops theoretical models for all three optical characteristics of microring modulator (λ_r, $\mathbb{Q}$ and ER), which are then extensively validated by the measured data.
- Models the BER as a function of the $\mathbb{Q}$ and the ER, and the modulation wavelength dutuning.
- Proposes a novel electrical tuning model, that includes a new power penalty term in order to keep a constant BER.
- Identifies an energy-efficient AC swing voltage for the microring modulator to balance the modulation energy and laser power.

2. BACKGROUND

Fig. 2 illustrates a common optically-interconnected 3D stack multi-core architecture (e.g., Corona [13]). Lasers gen-

SLIP '15, June 6, 2015. San Francisco, California, USA

erate light of multiple optical channels. Then the light propagates through a bus waveguide. As wavelength-selective devices, microring modulators can modulate light at a single optical channel. On the receiver side, light is directed by microring resonators and converted to electrical signals by photodetectors. Therefore, the wavelength-selective microring resonators and modulators play important roles in nanophotonic interconnects. In the following, we first describe the transmission spectrum model for passive microring resonators and then introduce two common types of active microring modulators.

2.1 Transmission Spectrum Model for Microring Resonators

The transmission spectrum of a microring resonator adjacent to a resonance wavelength λ_r can be described by a Lorentzian function [1]:

$$T(\Delta\lambda) = 1 - \frac{A}{1 + (2\mathbb{Q} \cdot \Delta\lambda/\lambda_r)^2} \quad (1)$$

where $\mathbb{Q}$ is the quality factor of the microring resonator defined as the ratio of the resonance wavelength to the full width at half maximum (FWHM) (Fig. 3). The extinction ratio (ER), another key characteristic of a microring resonator, is defined as $T_{max}/T_{min} = 1/(1-A)$. Fig. 1 (c) demonstrates that the Lorentzian spectrum model fits the measured data well.

Fig. 3 illustrates the tuning and on-off modulation scheme using a carrier-injection microring modulator. Due to fabrication-induced process variations and run-time temperature fluctuations, the modulator's resonance wavelength often deviates from the carrier wavelength [5]. A DC bias is usually applied to re-align the resonance wavelength to the carrier wavelength (from the spectrum T0 to T1), which is called electrical tuning (or bias voltage tuning) [5,11,12,14]. Then an AC modulation signal is applied to modulate the spectrum between T1 and T2. The optical power at logic "0" is $P_0 = P \cdot T_1(\Delta\lambda = 0)$ and at logic "1" is $P_1 = P \cdot T_2(\Delta\lambda = \Delta\lambda_m)$, where $\Delta\lambda_m$ is the wavelength dutuning between the spectra T1 and T2; P is the input optical power.

2.2 Modulation Mechanisms of Microring Modulators

Microring modulators use the plasma dispersion effect to change the silicon refractive index and then the microring resonance wavelength by changing the carrier concentration

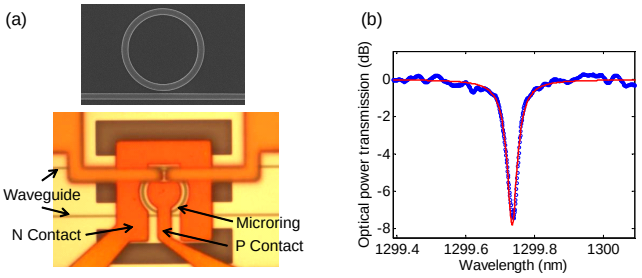

Figure 1: (a) The SEM (upper) and the microscopic (lower) image of a fabricated microring modulator; (b) The measured and model fitted optical transmission spectrum of a microring modulator.

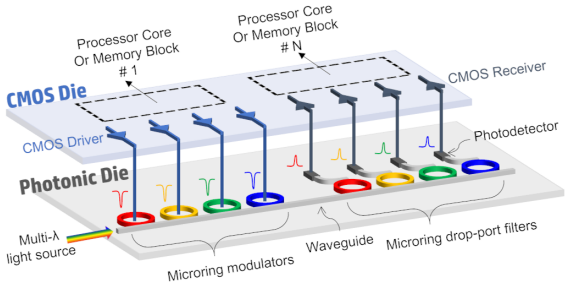

Figure 2: A 3D stack multi-core system using WDM nanophotonic interconnects.

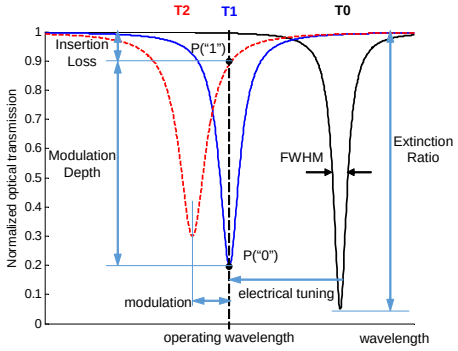

Figure 3: Modulation and tuning scheme of a microring modulator, where the spectrum T0 is at zero bias and the T1 and T2 are respectively transmitting logic "0" and "1".

in silicon [15]. Meanwhile, the optical loss coefficient of silicon increases with carrier concentration, which is considered as an undesired side effect. The plasma dispersion effect is quantified around 1.3 μm wavelength as following equations [15, 16] (The α below is the *amplitude* loss coefficient in unit of cm^{-1}, and is 1/2 of the power loss coefficient value reported in the references):

$$\Delta n = -(6.2 \times 10^{-22}\Delta N_e + 6.0 \times 10^{-18}(\Delta N_h)^{0.8})$$
$$\Delta\alpha = 3.0 \times 10^{-18}\Delta N_e + 2.0 \times 10^{-18}\Delta N_h \quad (2)$$

The change of carrier concentration can be achieved by either injecting or removing carriers, which leads to two common types of modulators: the carrier-injection type [17–20] and the carrier-depletion type [21–23]. In a carrier-injection p-i-n diode modulator (Fig. 4(a)), electrons and holes are injected into the intrinsic region when the junction is forward-biased. The carrier concentration within the waveguide core will increase and the silicon core's refractive index will decrease. Therefore, the resonance wavelength will blueshift. The I-V characteristics of the carrier-injection modulator can be well described by the equation $I = I_S e^{q(V-IR-V_t)/(nkT)}$ in [18], as shown in Fig. 4 (c) where n is the diode ideality factor.

In a carrier-depletion p-n diode modulator (Fig. 4(b)), the waveguide core is doped and a depletion region is formed near the p-n interface. When the junction is reverse-biased, the depletion region will be widened and carrier concentration in the core will decrease. Therefore, the silicon index

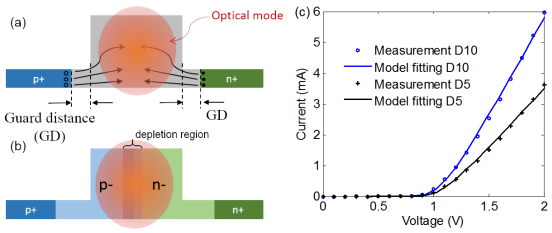

Figure 4: (a)(b) cross section views of a carrier-injection modulator and a carrier-depletion modulator, where the guard distance (GD) is the distance between the waveguide and the implantation region. (c) I-V characteristics of two carrier-injection modulators with diameters of 5 µm (D5) and 10 µm (D10).

will increase and the resonance wavelength will redshift.

3. OPTICAL SPECTRUM MODELS

3.1 Carrier-Injection Modulator

In a carrier-injection modulator, the microring spectrum is displaced and varied with injected current (Fig. 5 (a)). In this subsection, we derive and validate theoretical models for λ_r, ER and $\mathbb{Q}$, which together result in good agreement with measured spectra (Fig. 5 (a)).

The resonance wavelength shift is proportional to the effective index change: $\Delta\lambda_r = \lambda_r/n_g \cdot \Delta n_{eff}$,where $n_g = n_{eff} - \lambda \cdot dn_{eff}/d\lambda$ is the group effective index that accounts for the effective index dispersion. The $\Delta n_{eff} = \Gamma \Delta n_{Si}$, where Γ is the confinement factor describing the overlap of the optical mode with the silicon core [24]. Based on the plasma dispersion effect described in (2), there is an approximation $\Delta n_{Si} = -n_f \Delta N$ [17], where $n_f = 2.13 \times 10^{-21}\text{cm}^3$ around $\Delta N_h = 10^{18}\text{cm}^{-3}$, and $\Delta N = \Delta N_e = \Delta N_h$ is the electron-hole pair density in the junction. The dependence of the carrier concentration change ΔN_{inj} on injected current I can be derived from [18]:

$$\Delta N_{\text{inj}} = \frac{Q_0}{2q\mathbb{V}}\left(\sqrt{1+\frac{4I\tau_0}{Q_0}}-1\right) \tag{3}$$

where τ_0 is the carrier lifetime at a low carrier density, Q_0 is a fitting parameter describing the dependence of carrier lifetime on carrier density, and $\mathbb{V}$ is the junction volume. This *nonlinear* relationship will be shown to be vital in explaining the measured data.

By arranging the equations above, we derive the electro-optic (EO) effect induced $\Delta\lambda_r$ as:

$$\begin{aligned}\Delta\lambda_r^{EO} &= -\frac{\lambda_r\Gamma}{n_g} n_f \frac{Q_0}{2q\mathbb{V}}\left(\sqrt{1+\frac{4I\tau_0}{Q_0}}-1\right) \\ &\triangleq -a\cdot(\sqrt{1+I/I_0}-1)\end{aligned} \tag{4}$$

In a practical carrier-injection modulator, the thermo-optic effect caused by the joule heating of the injected current is non-negligible. The silicon index increases with temperature: $\Delta n_{Si} = dn_{Si}/dT \cdot \Delta T = 1.86 \times 10^{-4}\Delta T$. The temperature rise ΔT can be characterized as $\Delta T = \theta I^2 R$, where θ is the effective thermal impedance. Therefore, the thermal-effect-induced resonance wavelength shift is:

$$\Delta\lambda_r^{th} = \frac{\lambda_r\Gamma}{n_g}\frac{dn_{Si}}{dT}\theta R\cdot I^2 \triangleq c\cdot I^2 \tag{5}$$

By combining (4) and (5), we can express the total resonance wavelength shift as:

$$\Delta\lambda_r^{total} = -a\cdot(\sqrt{1+I/I_0}-1)+c\cdot I^2 \tag{6}$$

Equation (6) results in excellent fitting of the measured data of devices with various diameters (D), guard distances (GD) and from different fabrication batches as shown in Fig. 5 (b)(c) and Fig. 6. Since our model captures the *nonlinear* relationship between ΔN_{inj} and I, it shows significantly better fitting results than the empirical polynomial model ($\Delta\lambda_r = a\cdot I + b\cdot I^2$) in [6] that assumes *linear* $N_{\text{inj}} - I$ relationship. The Fig. 6 shows that our model greatly reduces the root mean squared (RMS) fitting error by 4X - 12X compared to the empirical polynomial model.

By comparing the Lorentzian model in (1) and the T-matrix model in [25], we relate the $\mathbb{Q}$ and ER to the optical loss by the following equations:

$$A = 1-\left(\frac{t-e^{-\alpha l}}{1-te^{-\alpha l}}\right)^2, \quad \mathbb{Q} = Q_c\frac{t^{1/2}e^{-\alpha l/2}}{1-te^{-\alpha l}} \tag{7}$$

where t is the portion of the optical field amplitude that remains in the original waveguide during the coupling between the straight waveguide and the microring, α is the *amplitude* loss coefficient within the microring, l is the ring circumference, and Q_c is a fitting coefficient for quality factor.

The optical loss α increases with the carrier concentration: $\alpha = \alpha_0 + \Delta\alpha = \alpha_0 + n_a\Delta N$, where α_0 is the loss coefficient at zero injection, and $n_a = \Delta\alpha/\Delta N = 5.0\times10^{-18}\text{cm}^2$ extracted from (2). The models above for ER (or A) and $\mathbb{Q}$ demonstrate good fitting results of the measured data (Fig. 5 (d)(e)).

3.2 Carrier-Depletion Modulator

By incorporating the depletion charge expression in an abrupt p-n junction, we express the $\Delta\lambda_r$ for the carrier-depletion modulator as:

$$\Delta\lambda_{r,\ dep} = \frac{\lambda_r\Gamma n_f}{n_g w_{wg}}\sqrt{\frac{2\epsilon}{q}\frac{N_aN_d}{N_a+N_d}}\left(\sqrt{V_{bi}-V}-\sqrt{V_{bi}}\right) \tag{8}$$

where w_{wg} is the waveguide width, N_a and N_d are the p and n doping concentration respectively, V_{bi} is the built-in bias voltage and $V(<0)$ is the external reverse bias voltage.

This proposed model is validated by the measured data extracted from [22], in which the device design parameters are: $w_{wg} = 0.5$ µm, $N_a = 5\times10^{17}\text{cm}^{-3}$ and $N_d = 1\times10^{18}\text{cm}^{-3}$ and the resonance wavelength is around 1550.7 nm. Our optical mode simulation shows $\Gamma = 0.77$ and $n_g = 3.98$, and the n_f is $4.26\times10^{-21}\text{cm}^3$ around $\Delta N_h = 1\times10^{17}\text{cm}^{-3}$. Based on these numbers, the $\Delta\lambda_r$ of the carrier-depletion modulator is calculated, which agrees well with the extracted measured data as shown in Fig. 5 (f).

4. SYSTEM-LEVEL MODELS AND IMPLICATIONS

Based on the established optical spectrum model, we derive analytical equations for the modulator power consumption and the transmission BER. Furthermore, implications

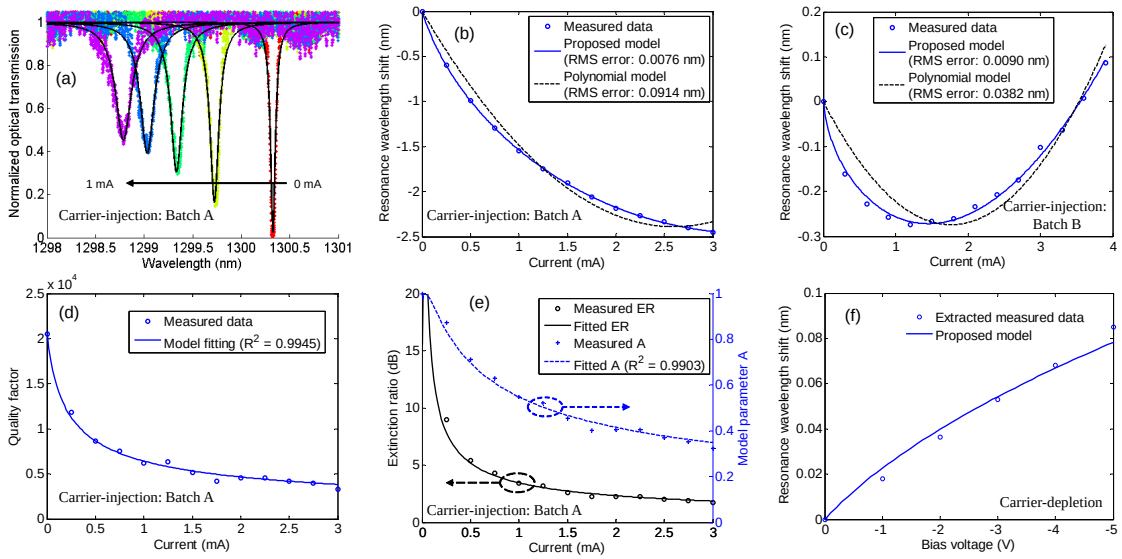

Figure 5: (a) Spectra series under injected current ranging from 0 to 1 mA, where dot: measured data, line: modulation model; (b)(c) $\Delta\lambda_r$ model fitting of carrier-injection modulators from Batch A and Batch B; (d)(e) $\mathbb{Q}$ and ER model fitting of a carrier-injection modulator; (f) calculated and measured $\Delta\lambda_r$ (extracted from [22]) in a carrier-depletion modulator.

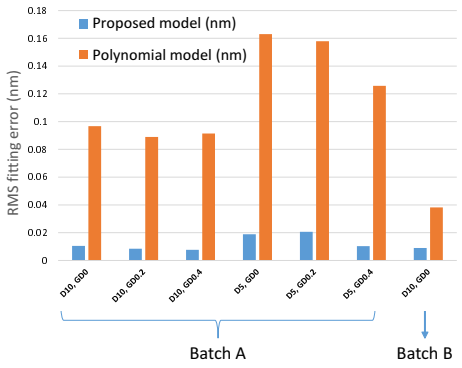

Figure 6: Root mean squared (RMS) fitting errors using our proposed model and the polynomial model, where D denotes diameter and GD denotes guard distance illustrated in Fig. 4 (a).

on the electrical tuning and the modulator swing voltage are discussed.

4.1 Power Model

The power consumption of the microring modulator consists of two parts: the static power consumption and dynamic energy consumption. The static power can be simply calculated by $I \cdot V$ by using the exponential I-V equation described in Section 2.2. The dynamic switching energy per bit is given:

$$E_{mod} = \frac{1}{4} V \Delta Q_m = \frac{V}{4} \frac{n_g q \mathbb{V}}{\lambda_r \Gamma n_f} \Delta\lambda_m \tag{9}$$

where ΔQ_m is the injected charge for switching; $\Delta\lambda_m$ is the wavelength detuning for switching.

4.2 Bit-Error-Rate Model

The dependence of the BER on the optical power levels at logic 1 and logic 0 is given by:

$$BER \approx 1/2 erfc(z/\sqrt{2}), \quad z = \frac{\rho(P_1 - P_0)}{\sigma_1 + \sigma_0} \tag{10}$$

where erfc is the complementary error function, z is a factor for modulation quality; ρ is the responsivity of the photodetector; P_1 and P_0 are the logic "1" and logic "0" corresponding optical power; σ_1, σ_0 are the corresponding noise standard deviation. Plug in the equations for P_1 and P_0 in Section 2.1, we obtain

$$z = \frac{\rho P}{\sigma_1 + \sigma_0} A \left(1 - \frac{1}{1 + (2\mathbb{Q} \cdot \Delta\lambda_m / \lambda_r)^2}\right) \tag{11}$$

where P is the optical power level without the insertion of the microring modulator. Thus, the BER, is related to the microring modulator characteristics (ER and $\mathbb{Q}$), and the modulation wavelength detuning $\Delta\lambda_m$.

4.3 Electrical Tuning Model

It has been shown in Section 3.1 that the Q and ER decrease significantly when the microring modulator is biased. Therefore, during the electrical tuning, the Q and ER would decrease and the BER would deteriorate. According to the (11), the optical power P must be increased in order to maintain a constant BER (or the factor z). Usually, the laser output optical power is increased to increase the optical power in the link. The increasing of laser output power is defined as the *power penalty* for the electrical tuning:

$$PP = P(A_1, \mathbb{Q}_1)/P(A_0, \mathbb{Q}_0) \tag{12}$$

where the subscripts "0" and "1" denote the ER (or $\mathbb{Q}$) before and after the electrical tuning, respectively. The power penalty is plotted as a function of resonance wavelength shift

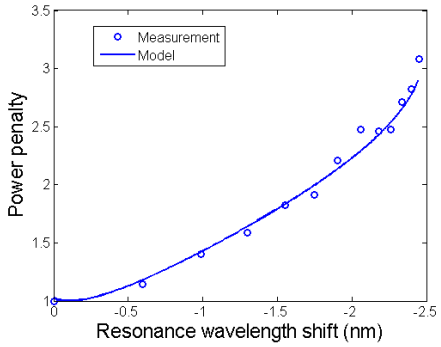

Figure 7: The power penalty for the electrical tuning as a function of tuning distance.

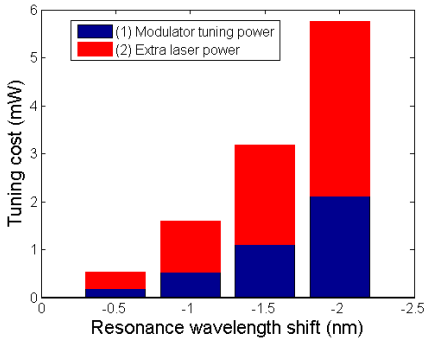

Figure 8: The total tuning cost for the electrical tuning as a function of the tuning distance. The link budget assumptions: receiver sensitivity: -17dBm @ 10^{-12} BER at 10 Gbps [26]; waveguide loss: 2.5 dB/cm; waveguide length: 1 cm; the silicon hybrid laser wall plug efficiency: 2% [27]

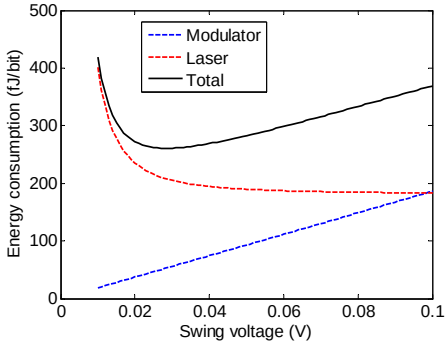

Figure 9: The energy consumption of the laser and the carrier-injection modulator as functions of the modulator AC swing voltage. The DC bias voltage is 1V. The energy consumption per bit of the laser is calculated at a 10 Gbps datarate.

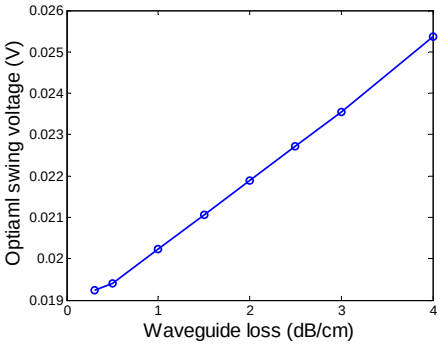

Figure 10: The energy-efficient swing voltage for a carrier-injection modulator as a function of the waveguide loss. Common waveguide loss values (0.3 - 4 dB/cm) are swept [28].

for a measured microring modulator in Fig. 7. For a common tuning distance of 1 nm [12], the power penalty is about 1.4, which means that the laser output power must be increased to 1.4 times in order to maintain the same BER as before tuning. The increasing of laser power poses additional overhead for the electrical tuning.

We propose that the total tuning cost for the electrical tuning should consist two parts: (1) the modulator tuning power ($I \cdot V$); (2) the extra laser power consumption due to the power penalty. The total tuning cost for electrical tuning as a function of the tuning distance is plotted in Fig. 8, which demonstrates that the extra laser power takes a significant portion of the total electrical tuning cost. As a result, the extra laser power must be considered as part of the electrical tuning cost in order to maintain a constant BER. In summary, the analysis of electrical tuning demonstrates the importance of our models for the $\mathbb{Q}$, the ER, and the BER.

4.4 Energy-Efficient Swing Voltage

The laser power consumption usually dominates the total power consumption of an optical link [11]. Hence, a large $\Delta\lambda_m$ is usually desirable for a low laser output power required to achieve the target BER (e.g., 10^{-12}), as indicated in (10) and (11). However, a large $\Delta\lambda_m$ will also leads to excess modulator energy, as shown in (9). Therefore, there is a trade-off between the laser power and modulation energy. Fig. 9 shows an energy-efficient AC swing voltage around 23mV in order to minimize the total energy consumption per bit. Furthermore, the energy-efficient swing voltage has a dependence on the waveguide loss (Fig. 10). As the waveguide loss increases, the laser power consumption takes a larger portion of the total power consumption. Consequently, a larger voltage swing is preferred to save the laser power.

5. CONCLUSION

In this paper, we develop theoretical optical spectrum models for microring modulators that includes all three optical characteristics (i.e. λ_r, $\mathbb{Q}$, and ER). The optical spectrum models are extensively validated by measured devices from various designs and fabrication batches, and demonstrate high fidelity. Based on the validated optical spectrum models, we derive the system-level models for power consumption and BER for microring modulators, which have dependence on optical characteristics ($\Delta\lambda_r$, $\mathbb{Q}$, and ER) and modulation swing voltage. Our model set has several design

implications for nanophotonic interconnects: In the electrical tuning, the optical power must be increased to compensate for the degradation of the $\mathbb{Q}$ and the ER to avoid the BER degradation. This increasing of optical power, or power penalty, is non-negligible and must be included in the total cost for the electrical tuning. In the AC modulation of the microring modulator, we identify an energy-efficient swing voltage to minimize the total energy consumption. Overall, our models for optical characteristics (λ_r, $\mathbb{Q}$, and ER), power and BER are important in accurate and comprehensive analysis of nanophotonic interconnects.

6. ACKNOWLEDGMENTS

The authors would like to thank Dr. Tsung-Ching Huang from HP Labs for his valuable advises. R. Wu and K.-T. Cheng acknowledge the Semiconductor Research Corporation for the support.

7. REFERENCES

[1] R. G. Beausoleil, "Large-scale integrated photonics for high-performance interconnects," *ACM Journal on Emerging Technologies in Computing Systems (JETC)*, vol. 7, no. 2, p. 6, 2011.

[2] Synopsys, "Optsim circuit product overview." `http://optics.synopsys.com/rsoft/rsoft-optsim-circuit.html`.

[3] Mentor Graphics, "Mentor graphics and lumerical unify optical design and simulation flow." `http://www.mentor.com/company/news/mentor-lumerical-optical-design`.

[4] Si2, "Silicon photonics technical advisory board (tab)." `http://si2.org/sptab-index.php`.

[5] Z. Li, M. Mohamed, X. Chen, E. Dudley, K. Meng, L. Shang, A. R. Mickelson, R. Joseph, M. Vachharajani, B. Schwartz, *et al.*, "Reliability modeling and management of nanophotonic on-chip networks," *Very Large Scale Integration (VLSI) Systems, IEEE Transactions on*, vol. 20, no. 1, pp. 98–111, 2012.

[6] Z. Peng, D. Fattal, M. Fiorentino, and R. Beausoleil, "CMOS-compatible microring modulators for nanophotonic interconnect," in *Integrated Photonics Research, Silicon and Nanophotonics*, 2010.

[7] Z. Peng, D. Fattal, M. Fiorentino, and R. Beausoleil, "Fabrication variations in soi microrings for dwdm networks," in *Group IV Photonics (GFP)*, Sept 2010.

[8] D. Ding and D. Z. Pan, "OIL: a nano-photonics optical interconnect library for a new photonic networks-on-chip architecture," in *International workshop on System level interconnect prediction*, 2009.

[9] J. Chan, G. Hendry, A. Biberman, K. Bergman, and L. P. Carloni, "PhoenixSim: A simulator for physical-layer analysis of chip-scale photonic interconnection networks," in *Design, Automation & Test in Europe Conference & Exhibition (DATE)*, 2010.

[10] M. Mohamed, Z. Li, X. Chen, A. Mickelson, and L. Shang, "Modeling and analysis of micro-ring based silicon photonic interconnect for embedded systems," in *Hardware/Software Codesign and System Synthesis (CODES+ISSS)*, 2011.

[11] C. Sun, C.-H. Chen, G. Kurian, L. Wei, J. Miller, A. Agarwal, L.-S. Peh, and V. Stojanovic, "DSENT: a tool connecting emerging photonics with electronics for opto-electronic networks-on-chip modeling," in *Networks on Chip (NoCS)*, 2012.

[12] Y. Zheng, P. Lisherness, M. Gao, J. Bovington, K.-T. Cheng, H. Wang, and S. Yang, "Power-efficient calibration and reconfiguration for optical network-on-chip," *Journal of Optical Communications and Networking*, vol. 4, no. 12, pp. 955–966, 2012.

[13] D. Vantrease, R. Schreiber, M. Monchiero, M. McLaren, N. P. Jouppi, M. Fiorentino, A. Davis, N. Binkert, R. G. Beausoleil, and J. H. Ahn, "Corona: System implications of emerging nanophotonic technology," in *Computer Architecture, International Symposium on*, 2008.

[14] A. Titriku, C. Li, A. Shafik, and S. Palermo, "Efficiency modeling of tuning techniques for silicon carrier injection ring resonators," in *Optical Interconnects Conference*, 2014.

[15] R. A. Soref and B. R. Bennett, "Electrooptical effects in silicon," *Quantum Electronics, IEEE Journal of*, vol. 23, no. 1, pp. 123–129, 1987.

[16] G. T. Reed and A. P. Knights, *Silicon Photonics: An Introduction*, pp. 101–102. John Wiley & Sons, 2004.

[17] Q. Xu, S. Manipatruni, B. Schmidt, J. Shakya, and M. Lipson, "12.5 gbit/s carrier-injection-based silicon micro-ring silicon modulators," *Optics Express*, vol. 15, no. 2, pp. 430–436, 2007.

[18] S. Manipatruni, K. Preston, L. Chen, and M. Lipson, "Ultra-low voltage, ultra-small mode volume silicon microring modulator," *Optics Express*, vol. 18, no. 17, pp. 18235–18242, 2010.

[19] C. Li, C. Chen, B. Wang, S. Palermo, M. Fiorentino, and R. Beausoleil, "An energy-efficient silicon microring resonator-based photonic transmitter," *Design Test, IEEE*, vol. 31, pp. 46–54, Oct 2014.

[20] C.-H. Chen, C. Li, A. Shafik, M. Fiorentino, P. Chiang, S. Palermo, and R. Beausoleil, "A WDM silicon photonic transmitter based on carrier-injection microring modulators," in *Optical Interconnects Conference*, 2014.

[21] P. Dong, S. Liao, D. Feng, H. Liang, D. Zheng, R. Shafiiha, C.-C. Kung, W. Qian, G. Li, X. Zheng, *et al.*, "Low Vpp, ultralow-energy, compact, high-speed silicon electro-optic modulator," *Optics Express*, vol. 17, no. 25, pp. 22484–22490, 2009.

[22] P. Dong, R. Shafiiha, S. Liao, H. Liang, N.-N. Feng, D. Feng, G. Li, X. Zheng, A. V. Krishnamoorthy, and M. Asghari, "Wavelength-tunable silicon microring modulator," *Optics Express*, vol. 18, no. 11, pp. 10941–10946, 2010.

[23] G. Li, X. Zheng, J. Yao, H. Thacker, I. Shubin, Y. Luo, K. Raj, J. E. Cunningham, and A. V. Krishnamoorthy, "25Gb/s 1V-driving CMOS ring modulator with integrated thermal tuning," *Optics Express*, vol. 19, no. 21, pp. 20435–20443, 2011.

[24] J. Bovington, R. Wu, K.-T. Cheng, and J. E. Bowers, "Thermal stress implications in athermal tio2 waveguides on a silicon substrate," *Optics express*, vol. 22, no. 1, pp. 661–666, 2014.

[25] A. Yariv, "Universal relations for coupling of optical power between microresonators and dielectric waveguides," *Electronics Letters*, vol. 36, no. 4, pp. 321–322, 2000.

[26] X. Zheng, D. Patil, J. Lexau, F. Liu, G. Li, H. Thacker, Y. Luo, I. Shubin, J. Li, J. Yao, *et al.*, "Ultra-efficient 10gb/s hybrid integrated silicon photonic transmitter and receiver," *Optics Express*, vol. 19, no. 6, pp. 5172–5186, 2011.

[27] C. Zhang, S. Srinivasan, Y. Tang, M. J. Heck, M. L. Davenport, and J. E. Bowers, "Low threshold and high speed short cavity distributed feedback hybrid silicon lasers," *Optics express*, vol. 22, no. 9, pp. 10202–10209, 2014.

[28] M. J. Heck and J. E. Bowers, "Energy efficient and energy proportional optical interconnects for multi-core processors: Driving the need for on-chip sources," *Selected Topics in Quantum Electronics, IEEE Journal of*, vol. 20, no. 4, pp. 332–343, 2014.